



Bending tests on building beams containing electric arc furnace slag and alternative binders and manufactured with energy-saving placement techniques

Amaia Santamaría^a, Aratz García-Llona^b, Víctor Revilla-Cuesta^c, Ignacio Piñero^d,
Vanessa Ortega-López^{c,*}

^a Department of Mechanical Engineering, University of the Basque Country, UPV/EHU, Spain, Escuela de Ingeniería de Bilbao, I (bloque B) - UPV/EHU, Plaza Ingeniero Torres Quevedo, 1, 48013 Bilbao, Spain

^b Fundación Centro Tecnológico de Componentes, Parque Científico y Tecnológico de Cantabria, Calle Isabel Torres, 1, 39011 Santander, Cantabria, Spain

^c Department of Civil Engineering, University of Burgos, Spain, Escuela Politécnica Superior, Calle Villadiego s/n, 09001 Burgos, Spain

^d TECNALIA, Basque Research and Technology Alliance (BRTA), Parque Científico y Tecnológico de Bizkaia, Astondo Bidea, Edificio 700, 48160, Derio (Bizkaia), Spain

ARTICLE INFO

Keywords:

Waste management
Waste recycling
Electric arc furnace slag
Supplementary cementitious materials
Energy-saving concrete mixes
Building beams
Full-scale bending test on beams

ABSTRACT

The environmental impact of the building sector is especially relevant during the construction phase. Both the materials and the construction methods that are currently in use must be reconsidered, in order to minimize the environmental impact of concrete-based structures. This research is therefore focused on achieving greener concrete-based building structures. In this context, the feasibility of careful use of materials for concrete manufacture and the use of construction techniques that can facilitate and reduce energy consumption during placement are both studied. To do so, twelve sample beams were prepared using eight different sustainable high-workability structural concretes. The aim was to maximize the use of the by-products that amounted to over 80% of the concrete mass, steelmaking slags, fly ash, and quarry waste, and to employ energy-saving concrete placement techniques. The beams underwent bending tests in which their mechanical behavior and their compliance with the specifications of the most relevant building codes were verified. The results pointed to the feasibility of increased sustainability in the field of building engineering through the suitable use of selected by-products and techniques.

1. Introduction

Nowadays, the sustainability of human activity represents an unavoidable demand. According to the Brundtland Report, “Sustainable development is development that meets the needs of the present without compromising the ability of future generations to meet their own needs” [1]. The concept of the circular economy is now generalized in the planning processes of human activity [2]. In this way, scientific and technical works have sought to address the re-use of many and varied residual materials [3].

The penetration of the sustainability concept into the construction sector can imply short-term and long-term global benefits [4]. In the short-term, the use of certain waste-products as innovative construction materials has brought with it technical and economic benefits [5,6]. In

the long-term, intense consumption of natural resources (raw materials, energy) can be mitigated by using copious amounts of waste-products and by-products from industrial sectors [7], while maintaining a sufficient level of quality in the manufactured concrete components [8,9]. Scientific researchers are therefore proposing new, reliable, and beneficial substitutions [10,11]. The examples of by-products and wastes which can be reused in the construction industry are numerous [12,13]; among which, bottom ash [14,15], fly ash [16], construction and demolition wastes [17,18], and metallurgical slags [19,20] stand out.

Electric arc furnace slag (EAFS, also referred to as acid slag, oxidizing slag, or black slag from electric steelmaking) is an abundant by-product generated in the first stage of steel manufacturing when smelting down ferric scrap [21,22] that approximately yields 0.17 tons of slag per ton of steel [23,24]. The characteristic attractions for this material in

* Corresponding author at: Civil Engineering Department, EPS University of Burgos, Calle Villadiego s/n, 09001 Burgos, Spain.

E-mail addresses: amaia.santamaria@ehu.es (A. Santamaría), agl0053@alu.ubu.es (A. García-Llona), vrevilla@ubu.es, vortega@ubu.es (V. Revilla-Cuesta), ignacio.pinero@tecnalia.com (I. Piñero), vortega@ubu.es (V. Ortega-López).

<https://doi.org/10.1016/j.istruc.2021.04.003>

Received 24 December 2020; Received in revised form 21 March 2021; Accepted 7 April 2021

Available online 20 April 2021

2352-0124/© 2021 The Authors. Published by Elsevier Ltd on behalf of Institution of Structural Engineers. This is an open access article under the CC BY-NC-ND

license (<http://creativecommons.org/licenses/by-nc-nd/4.0/>).

constructional uses are its toughness [25,26], wear resistance [27,28], good durability [29,30], and superficial roughness [31,32]. The slightly higher density of this by-product in comparison with other alternative products can be seen as either an advantage or a disadvantage. Its superficial roughness and high density are disadvantageous for high-workability concretes, although this problem can be solved by correct dosing of the fines content in the concrete mix [33,34]. This high density is also a drawback for EAFS concrete elements to be self-supported or supported by other structural elements. However, if EAFS is used in concrete elements that require high stability, such as retaining walls and foundations, then high density can be considered an advantage [35]. Another common problem of EAFS is a slight risk of expansion, which can be reduced through suitable weathering processes [36,37]. Nevertheless, not all steel slags undergo expansion [38,39] and the varied chemical compositions of EAFS rule out any generalization of its expansiveness. Furthermore, certain by-products from steelmaking activities other than EAFS, such as ladle furnace slag (LFS) [40], are also useful in these sorts of construction sector applications [41,42].

Ground granulated blast-furnace slag (GGBS) is an ironmaking by-product added to concrete mixes as a Supplementary Cementitious Material (SCM) under specific conditions (marine environments, gypsum presence...). Nevertheless, its use is not popularized in the most common construction applications, *i.e.*, in the building sector. In fact, almost no GGBS is used in construction applications around the world [43]. On the other hand, fly ash (FA), a by-product of coal combustion, is frequently added to concrete binders as an SCM, although its use is nowadays decreasing, due to the closure of coal-fired power plants. Using these two by-products as binders will contribute to the reduction of conventional Portland cement production and consumption levels, thus promoting the circular economy and the sustainability of the building sector.

Limestone fines are another useful and often misused by-product that are also suitable for concrete production. Mined from quarries, the limestone undergoes a crushing process where the main commercial product is limestone gravel, a product that is widely used in civil works. However, limestone fines are extracted in excess of the quantities that are commercially required, so this product is often heaped around the quarry site. Nevertheless, these fines could be used more extensively in certain dry concrete mixes to enhance their workability, a common problem in EAFS concrete, implying economic savings and contributing to global sustainability [44].

The validity of these alternative materials for the production of concrete used in structural applications has mainly been studied in terms of the influence of each material within concrete specimens, and the mechanical behavior and the durability of the specimens [32,45]. Therefore, there is a notable lack of knowledge in relation to the validation of concretes made with these by-products in full-scale structural elements. Only the work of two research groups has dealt with these aspects, focusing mainly on the effect of EAFS on conventional vibrated concrete:

- Firstly, it is worth mentioning the pioneering authors from Korea (University of Kongju) and their papers on the behavior of reinforced-concrete (RC) beams manufactured with EAFS as aggregate [46–48]. The above-mentioned authors analyzed the bending strength of RC beams, observing comparable behaviors between both EAFS concrete and ordinary concrete. Their research was completed with a study on the bonding behavior of the reinforcement bars [49].
- Likewise, a team of authors from the University of Padua (Italy) studied the bending and shear failure of EAFS-RC beams and other structural features [50,51], showing that ultimate bending and shear capacities were higher in beams manufactured with EAFS concrete compared with beams manufactured with natural aggregate concrete. The same team found similar results when studying the local bonding strength between reinforcement bars and EAF slag concrete [52].

1.1. Significance and scope of this article

The aim of this paper is to evaluate the bending behavior of full-scale RC beams made not only with EAFS, but also with alternative binders such as GGBS and FA. Furthermore, in these beams different techniques were applied to concrete, to reduce energy consumption during placement (self-compactability or pumpability) [45,53–55] and to increase its toughness without increasing its binder content (fiber-reinforcement) [56–58]. This set of original and innovative conditions is a novel contribution both to the literature and in engineering practice. This study aims to show that concretes made with these alternative materials and techniques are valid for use in real structural elements.

In the present paper, the authors report an experimental work on their assessment of the use of electric arc furnace slag (EAFS) [59], other aggregate by-products [60], and alternative binders (SCM) [61], for the manufacture of concrete building components [62,63]. These by-products were always added in proportions higher than 80% by weight of all mix components (only clinker and water are out of this scope), and the pieces subsequently underwent rigorous mechanical tests to determine their behavior and usefulness.

Several kinds of medium-strength concretes, such as self-compacting concrete, pumpable concrete, and fiber-reinforced concrete containing electric arc furnace slag as aggregate, were employed to gain a broad overview of their performance as load-bearing elements supporting bending loads. In the following sections, the properties of some components, the mix compositions, and the beam casting process are described.

“EAFS concrete” beams, 4400 mm in length and around 0.7 tons in weight, containing steel ribbed bars both as longitudinal and transversal reinforcements, were tested for deformation and deflection [64]. Strength evaluations under four-point bending stress tests [65] were performed and the experimental results were compared with the specifications of standard calculation codes [66,67] to evaluate the suitability of those codes in relation to the EAFS beams. Their behaviors both under an elastic regime and at failure were studied to provide an overview of beam behavior under different loading conditions.

2. Materials and mixtures

2.1. Cement

Four types of cement were tested: firstly, a Portland cement-type I 52.5 R; secondly, a Portland cement-type IV/B-V 32.5-N containing 50% FA; thirdly, a Portland cement-type II/B-S 42.5-N containing 30% GGBS; and finally, a Portland cement-type III/B 32.5-N containing 70% of GGBS. All of these types were in conformity with the EN 197–1 European standard “*Cement - Part 1: Composition, specifications and conformity criteria for common cements*”, at which the designation of the cements throughout the paper refers [68]. Except for the type I 52.5-R cement, the other binders were Portland clinker mixed with active additions such as fly ash (FA-V), and ground granulated blast-furnace slag (GGBS-S), sourced from industrial by-products, which when reused will contribute to the circular economy and to sustainability goals. Furthermore, a small fraction (5% of total binder) of ladle furnace slag (LFS) [41] was added to the IIIP mix as a “minor additional constituent” of Portland cement.

2.2. Admixture, water, natural aggregates and EAF slag

The admixture consisted of a carboxylate-based water emulsion (a plasticizer and a viscosity conditioner agent) supplied by CHRYSO®™, whose main characteristic is its excellent compatibility with the EAFS aggregate. The results in terms of the self-compacting mixes were satisfactory. Mix water, containing no compounds with adverse effects on reinforced concrete, was taken from the urban mains supply (chlorine 1 ppm) of the city of Burgos, Spain.

Natural limestone fines from gravel crushing (sized in the interval 0/

Table 1
Mix proportions in kg per cubic meter of concrete.

Components	Batch 1				Batch 2		
	IP	IVP	ISC	IVSC	IISC	IISC-M/ IISC-Y	IIIP-M
Cement I 52.5R	330		330				
Cement IV/B-V 32.5 N		320		320			
Cement II/B-S 42.5R					330	330	
Cement III/B 32.5 N							320
Water	160	160	170	170	170	180/ 185	160
Medium EAFS (4/12 mm)	980	980	770	770	750	750	930
Fine EAFS (0/4 mm)	690	690	550	550	550	550	690
Limestone fines (<1.18 mm)	650	650	900	900	950	950	650
Admixture (% cement weight)	1.5	1.5	2.0	2.0	1.6	1.6	1.4
Fiber reinforcement (type-kg)						M-40/ Y-4.5	M-30
Total weight	2815	2805	2725	2715	2700	2740/ 2705 (*)	2780

Roman numerals I, II, III, and IV refer to the type of Portland cement in use, in accordance with EN-197-1 [68].

P = pumpable concrete; SC = self-compacting concrete; M = metallic fibers; Y = synthetic fibers.

(*) = the proportioning of these two mixes in the table amounts 1030 L.

2 mm, specific gravity 2.65 Mg/m³) with a fineness modulus of 1.5 units were used as complementary fine aggregate. As detailed in previous publications by the authors [34,69], this aggregate was added to coarse and fine EAFS to improve concrete workability up until the consistency required by self-compacting mixtures.

Electric arc furnace slag (EAFS) in two size fractions (fine < 4 mm, medium 4/12 mm), supplied by the company Hormor-Zestoa, was used in this research after crushing and three months spontaneous weathering. Their respective fineness moduli were 3.9 units for the fine fraction, and 5.7 units for the medium fraction. Details on this material may be found elsewhere in a previous publication from the authors [34].

2.3. Rebars and fibers

Conventional ribbed steel bars of several diameters (Ø25 mm, Ø16 mm, and Ø8 mm) were used as longitudinal tensile and compressive reinforcements, and Ø8-mm bars were used as transversal-shear reinforcement stirrups in the beams. The ribbed steel reinforcement was manufactured with B 500 S quality steel, in accordance with the specifications of standard UNE 36068 [68]. It is worth mentioning, as relevant data on this steel, a theoretical yield strength of 525 MPa and a

Table 2
Hardened properties of the mixes.

Batch	Mixture	Dry density (Mg/m ³)	90-day modulus of elasticity (GPa)	90-day Poisson's coefficient	Compressive strength after 7–28–90–180–360 days in a moist room (MPa)	Compressive strength from core drill (MPa)	
1	IP	2.71	38.6	0.23	42–53–63–64–64	67	
	IVP	2.62	31.4	0.22	18–29–36–48–56	41	
	ISC	2.60	39.9	0.22	42–53–66–76–77	72	
	IVSC	2.52	33.8	0.21	19–31–37–55–62	62	
2a	IISC	2.63	40.2	0.23	47–59–75–76–78	74	
	2b	IISC-M	2.57	34.7	0.22	38–53–63–65–69	63
		IISC-Y	2.54	31.6	0.22	33–46–57–59–61	61
		IIIP-M	2.65	26.1	0.19	20–27–33–38–42	34

theoretical yield strain of 4.5‰ (strain formula given in equation (1)). In this work, the Young's modulus of the steel (E_s) will be considered equal to 210 GPa.

$$e_y = 2 + \frac{525}{E_s} \tag{1}$$

Both metallic (M) and synthetic (Y) fiber types were separately used in three different mixes of EAFS concrete, to assess their efficiency at interacting with the surrounding cementitious matrix. The steel fibers were end-shaped wire pieces type HE-55/35 with a length of 35 mm, a diameter of 0.55 mm, a tensile strength of 1200 MPa and a density of 7900 kg/m³. The polypropylene type T-35 fibers were surface-dimpled pieces of 35 mm in length and 0.93 mm in diameter, with a tensile strength of 400 MPa, an elastic modulus of 6 GPa, and a density of 910 kg/m³.

2.4. Mix design and relevant in-fresh characteristics.

Eight different concrete mixes containing EAFS slag as the major aggregate were prepared to perform twelve beams. The mix compositions and properties have been fully detailed elsewhere by the authors [70]. Three of the mixes were “pumpable” concretes (mixes for on-site pumping) and the other mixes (five) were self-compacting mixes.

As shown in Table 1, the mixes were divided into two groups or batches. Batch 1 corresponded to four mixes (and four beams manufactured in 2017), mixed with cement types I and IV. Batch 2 corresponded to four mixes (and eight beams manufactured in 2018), which were performed using Portland cements type II and III, both mainly based on GGBS. It is worth mentioning the use of ribbed bars of two different diameters (Ø16 and Ø25 mm) in Batch 2 for longitudinal reinforcement, and the additional use of reinforcing fibers (metallic M, synthetic Y) in three of the mixes.

The cement amount (320–330 kg/m³), and the w/c ratio (around 0.5 units) were usual values in structural concrete mixtures to obtain a universally accepted compressive strength for medium structural concrete (30 to 50 MPa at 28 days in moist-room-conserved specimens). Workability was planned in pumpable mixes as a target slump of 200 mm, and in self-compacting mixes as a target spread on a flat plate of 600 mm within around five seconds (both tested using the Abrams cone). The mix proportioning is shown in Table 1 for the in-fresh mixes. Any slight grading differences between dosages were corrections, due to differences between the components of the two batches (binder, fibers, aggregates...).

The pumpable-type mixtures (IP, IVP, IIIP-M) achieved an S4 consistency slump class in the Abrams cone test. When pouring formwork, these pumpable mixtures showed acceptable flowability, with a need for some slight formwork vibration. Some of the self-compacting mixtures (ISC, IVSC, IISC) achieved an SF2 slump class, spreading beyond 660 mm, but the presence of fibers decreased the flowability of the fresh concrete in mixes IISC-M and IISC-Y that achieved an SF1 slump class.

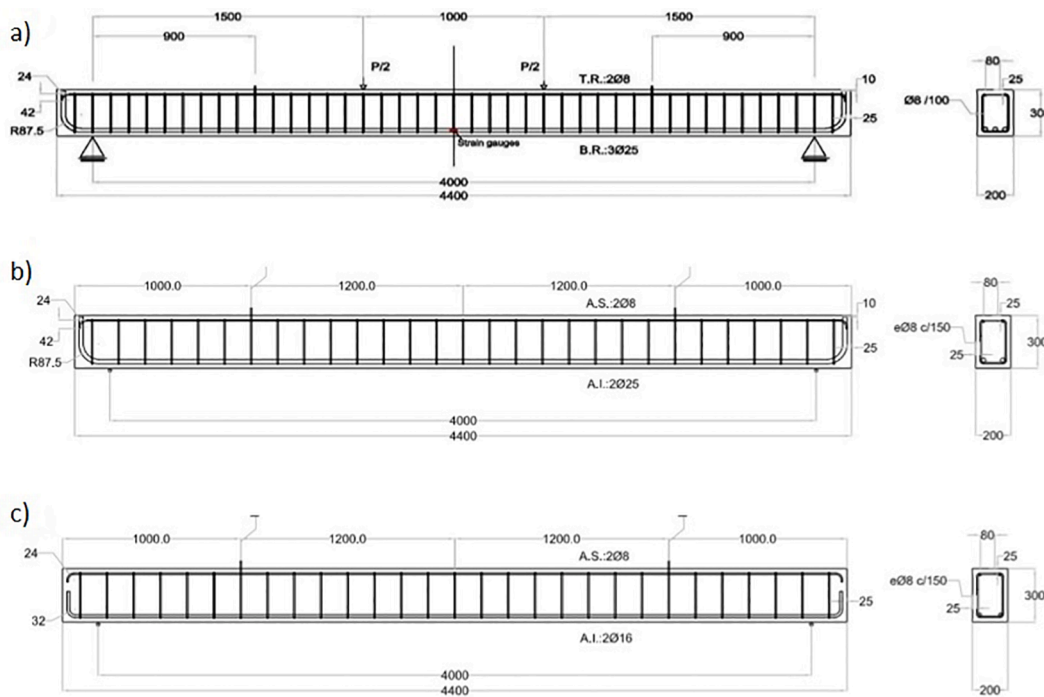


Fig. 1. Beam reinforcement details: a) type I and IV (Batch 1) concrete; b) type II and III (Batch 2) concrete; c) type II and III (Batch 2) concrete.

3. Properties of hardened mixtures

The most relevant mechanical properties of the mixtures used in this work in terms of strength and stiffness are presented in Table 2. These results were obtained from testing 100 × 200-mm cylindrical specimens conserved over one year in a moist room (20 °C and 98% relative humidity). The concrete dry densities varied from 2.52 to 2.71 Mg/m³.

With regard to concrete compressive strength at early ages (until 28 days), the mixtures can be divided into two classes according to the type of cement. So, the mixes manufactured with cement types III and IV and large amounts of pozzolanic materials (70% GGBS, 50% FA) reached over 30 MPa after 28 days in a moist room, while the mixes manufactured with cement types I and II reached over 50 MPa at the same curing age. The subsequent evolution of compressive strength over one year led to final values in the order of 60-to-78 MPa in six of the mixes, while the mixes with the highest additions of supplementary cementitious materials remained among the lowest values 42–56 MPa. It must therefore be recalled that these results were obtained from carefully conserved specimens held in a standardized moist room. The properties of the concrete beams, weathered for over two years in the testing shed (indoor environment), might differ from the above-mentioned conditions.

Measurements of the elastic properties, the Young’s moduli and the Poisson’s coefficients were taken on cylindrical specimens after 90 days of moist room curing. The mixtures manufactured with cement types I and II showed linear elastic fields with slopes (Young’s modulus) in the range of 35 to 40 GPa, and those manufactured with cements III and IV showed Young’s moduli of 26–34 GPa, as can be seen from Table 2. The Poisson’s coefficients were in almost all cases 0.22 units, except in the

type III cement mix, in which the value descended to 0.19 units. This last circumstance is usually associated with a higher deformability-ductility of the cementitious material at the moment of plastic failure.

In the last column of Table 2, the results of the compressive tests on the core-drilled specimens are displayed. The specimens were obtained from real sections, one year after the bending tests described in the following sections, in a transversal direction with respect to the main beam axis. The spontaneous aging of concrete in the testing shed was extended beyond one year. It was evident that the differences between these values and the values of the specimens conserved in a moist room were not pronounced. In general, it was accepted that the real compressive values of the concrete after one year will be a good proxy of the results after 90–180 days in a moist room.

4. Bending tests

4.1. Specimen details and test setup

A set of twelve beams were poured for this experimental campaign of bending tests, identifying the type of concrete (mixtures described in Batches 1 and 2) and the type of longitudinal reinforcement. The denomination of each beam contained the information on the concrete characteristics and on the amount of reinforcement. The nominal dimensions of all beams were 200 × 300 × 4400 mm, as shown in Fig. 1, with a weight of 0.7 Tons.

Three types of reinforcement were used in the concrete beams, as depicted in Fig. 1. In all four beams from Batch 1, the longitudinal and transversal reinforcements (Fig. 1a, Table 3) consisted of 3Ø25 bars and

Table 3
Reinforcement characteristics and beam labels.

Batch	Mixtures	Reinforcement			Beams			
		Top	Bottom	Stirrups				
1	Type I and IV mixes	2Ø8	3Ø25	Ø8/100 mm	IP/25 or IP	IVP/25 or IVP	ISC/25 or ISC	IVSC/25 or IVSC
2a	Type II and III mixes	2Ø8	2Ø25	Ø8/150 mm	IISC/25	IISC-M/25	IISC-Y/25	IIP-M/25
2b	Type II and III mixes	2Ø8	2Ø16	Ø8/150 mm	IISC/16	IISC-M/16	IISC-Y/16	IIP-M/16

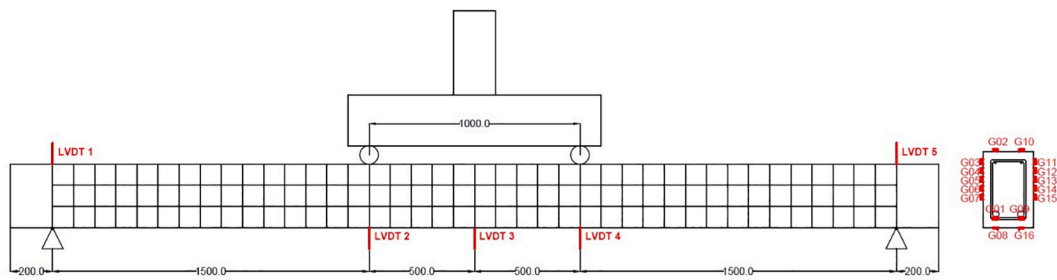


Fig. 2. Test setup details and measurement devices: longitudinal detail (left); transversal detail (right).



Fig. 3. Bending test setup.

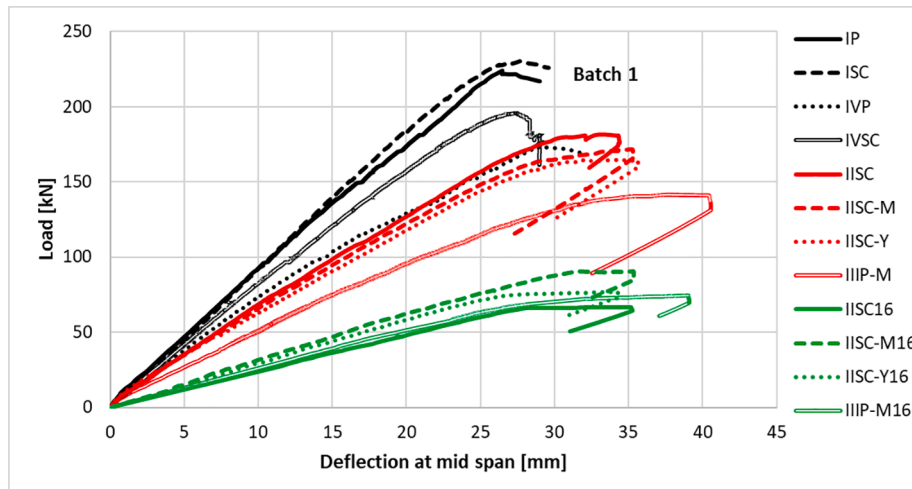


Fig. 4. Load-deflection curves of the three batches in the bending tests.

Ø8 stirrups every 100 mm, respectively.

The main features of the Batch 2 concrete mixtures were their longitudinal reinforcements: a first set of four beams with 2Ø25 bars, and a second set of four additional beams with 2Ø16 bars (Fig. 1, Table 3). In both cases, the beams had transversal Ø8 stirrup reinforcements every 150 mm.

Four-point tests were performed to evaluate the bending strength of the beams, as detailed in Fig. 2. All the beam spans measured 4000 mm. The three partial spans measured 1500–1000–1500 mm. The central span was in a state of pure bending, without shear forces, supported by the transversal reinforcements of the lateral spans.

Two comparator clocks and five LVDTs were positioned (see Fig. 3)

along the beam span to measure the displacements of its main (supported, center and loading) sections. Additionally, sixteen strain gauges were positioned on all four faces (lateral and horizontal) within the central section to measure concrete strain, and on the longitudinal steel bars, as depicted in Fig. 2. The position of the neutral axis and the strain at several positions supplied relevant data for the global analysis of the results. One datum per second was relayed from the instruments (five LVDTs, 16 strain gauges, load cells and comparators) during the test to record the variables: temperature, loading and deflection displacements. The information from the comparator gauges was manually noted on paper.

The beams were tested, having cured for several months (from 8 to

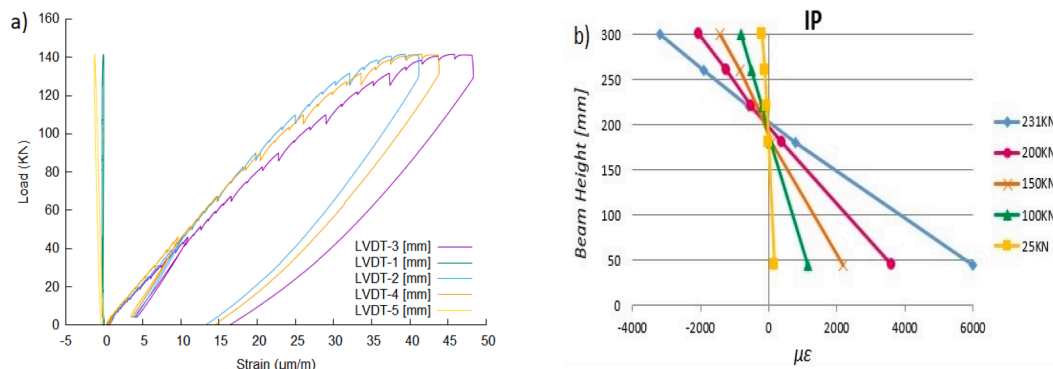


Fig. 5. Real examples: a) load–deflection curves of IIP-M/25; b) strain profiles of IP/25 beam.

12) in the University of Burgos testing shed. Prior to recording the definitive test data, the beams were loaded and unloaded above the concrete tensile cracking load (around 5 kN). Hence, the initially higher slope of linear behavior before the onset of tensile cracking was omitted from the curves. The beams were tested until failure, i.e., beyond the ultimate strength load shown in the curves.

4.2. Experimental results of bending tests

In Fig. 4, the curves of the four beams from each Batch (1, 2a, and 2b) are depicted, in terms of total applied load versus LVDT-3 displacement measurements (maximum deflection, produced in the central section of the beam). The curves of each batch differed, due to three different aspects:

- Small geometric differences in beam dimensions and in test execution.
- Differences in the quality of the concrete.
- The presence-absence of fiber reinforcement, assuming that the rest of the conditions were the same.

Nevertheless, additional and unexpected differences appeared, for instance in the quality of the reinforcement steel, which are in each case commented upon below.

As may be expected, in well-performed structural concrete beams, previously subjected to slight loading up until tensile cracking on the underside of the concrete region, the general behavior showed an initial linear elastic region: material stiffness and the static test conditions determining the slope. This behavior was observed up until approximately 80% of the failure load. Afterwards, a non-linear region with a decreasing slope extended to a maximum, denoting the yield points of some of the materials. The peak of the curve reflects the moment of beam failure.

Regarding the Batch 1 curves (Fig. 4), it can be seen that both the IP and the ISC beams, of very similar concrete quality, showed similar global behaviors. The curve of the IVSC beam, beneath both, was due to its slightly lower concrete quality, and the curve of the IVP beam was the lowest in the batch. The reference properties for the above comparison, shown in Table 2, were concrete stiffness and strength measured on specimens conserved for 28 or 90 days in a moist room.

In both Batch 2a and 2b, the corresponding beams were manufactured in parallel (two by two) and poured at the same moment using a single concrete mix. The curves of mixtures IISC, IISC-M and IISC-Y (in that order) showed the strongest beams, and at the other extreme, the IIP-M beam was the weakest. All the data are shown in Table 2. In Batch 2b, some additional circumstances to those mentioned for the batch 2a beams caused some erratic results, which are displayed in Fig. 4. The different effect of fibers in both batches meant that no clear beneficial effect of the fiber additions could be established: neither increased

bending stiffness nor increased ultimate failure loads. A result that the lower compressive strength and elastic stiffness can explain, which are due to the higher water content that is required when adding fibers to preserve the workability of the concrete mixes [53].

A real example of the coarse data from the data-acquisition system on a representative test (for instance, IIP-M/25 beam) is depicted in Fig. 5a. Five LVDTs were set in position, two (LVDT 1, and 5) at the supports, and three (LVDT 2, 3, and 4) within the central region subjected to a constant bending moment. Rigorous filtering of values was completed to obtain the final curves in Fig. 4. Fig. 5a shows the initial load-unload cycles (beam IIP-M/25), and the subsequent steps of the beam-cracking test, used to study cracking within the beam. Fig. 5b shows an example (beam IP/25) of the horizontal strain profiles (corresponding to several load levels throughout the test) in the central section of the beam, drawn from the average data taken by strain gauges G2 to G7 and their counterparts G10 to G15. Twelve similar graphics were obtained for the twelve beams.

4.3. Bending analysis under an elastic regime

The maximum deflection of a four-point loaded beam is described in the literature on material elasticity and strength with Eq. (2), where l is the span length, P and a are half-measures of load and lateral span, and δ is the deflection measured in the center of total span. Equation (4) was used to calculate the bending compliance, c , of that piece, in terms of total load (P_T , Eq. (3)) and central section deflection (δ , Eq. (2)). In Equation (5), E is the Young’s elastic modulus of the concrete in GPa (kN/mm^2) and I is the effective moment of inertia reduced to concrete (using the n ratio for steel) and measured in mm^4 . This equation yielded a compliance value, using mm and kN as units, and considering that l and a are equal to 4000 mm and 1500 mm, respectively. According to the experimental data (Section 4.2), this formula, suitable for elastic behavior, appeared to be valid up until 80% of the failure load.

$$\delta = \frac{(3 \cdot l^2 - 4 \cdot a^2) \cdot P \cdot a}{24 \cdot E \cdot I} \tag{2}$$

$$P_T = 2 \cdot P \tag{3}$$

$$c = \frac{\delta}{P_T} = \frac{(3 \cdot l^2 - 4 \cdot a^2) \cdot a}{48 \cdot E \cdot I} \tag{4}$$

$$c \left(\frac{\text{mm}}{\text{kN}} \right) = \frac{1.21875 \cdot 10^9}{E \cdot I} \tag{5}$$

Continuing with the elastic analysis of the beam sections, two variables are usually estimated: the position-depth of the neutral axis and the effective moment of inertia. The depth of the neutral axis (x^{NA}) was obtained with a second-degree equation, Eq. (6), based on the equality of static moments of the upper and the lower areas, using the simplified

Table 4
Elastic regime calculations.

Batch	BEAM	Initial values		Results of calculation			Experimental data		Corrected values	
		90-day E (GPa)	n	Neutral axis depth, x^{NA} (mm)	I (mm ⁴)	Compliance c (mm/kN)	Compliance c (mm/kN)	Neutral axis depth, x^{NA} (mm)	n	I (mm ⁴)
1 (3Ø25)	IP	38.6	5.5	108	275e + 06	0.116	0.106	110	–	–
	IVP	31.4	7.0	118	322e + 06	0.126	0.152	141	12	452e + 06
	ISC	39.9	5.5	108	275e + 06	0.116	0.111	106	–	–
	IVSC	33.8	6.0	112	292e + 06	0.119	0.120	117	–	–
2a (2Ø25)	IISC/25	40.2	5.5	93	206e + 06	0.155	0.157	93	–	–
	IISC-M/25	34.7	6.0	96	220e + 06	0.158	0.165	97	–	–
	IISC-Y/25	31.6	7.0	102	246e + 06	0.165	0.172	104	–	–
	IIIP-M/25	26.1	8.0	107	270e + 06	0.171	0.212	131	15	410e + 06
2b (2Ø16)	IISC/16	40.2	5.5	64	103e + 06	0.310	0.413	84	20	280e + 06
	IISC-M/16	34.7	6.0	67	111e + 06	0.314	0.310	68	–	–
	IISC-Y/16	31.6	7.0	71	126e + 06	0.322	0.340	71	–	–
	IIIP-M/16	26.1	8.0	75	140e + 06	0.331	0.390	85	15	230e + 06

“–” = unnecessary correction.

version in which ρ_2 is approximate to zero under compression. There, d is the effective beam height, equal to 260 mm, n (Eq. (7)) is the ratio of both the steel and the concrete Young’s moduli, and ρ_1 and ρ_2 are the geometric amounts of reinforcement under both tension and compression calculated according to Eq. (8), where A_i is the area of longitudinal reinforcement steel. The moment of inertia is expressed in this simplified version by Eq. (9). The literature contains more complete formulations when A_2 and ρ_2 are higher than 0 in the upper reinforcement but, in all cases, the main variables of the (concrete and steel) materials are stiffnesses (E_c and E_s) or their ratio (n).

$$\frac{x^{NA}}{d} = n \cdot \rho_1 \cdot \left(-1 + \sqrt{1 + \frac{2}{n \cdot \rho_1}} \right) \tag{6}$$

$$n = \frac{E_s}{E_c} \tag{7}$$

$$\rho_i = \frac{A_i}{b \cdot d} \tag{8}$$

$$I = n \cdot A_1 \cdot (d - x^{NA}) \cdot \left(d - \frac{x^{NA}}{3} \right) \tag{9}$$

The calculations of neutral axis depth (x^{NA}) and the inertia moment (I) of the reinforced section in the elastic regime must be based on realistic data. Assuming that it is not easy to ascertain the exact value of the Young’s moduli of these mixtures at the time of the bending test (a value which evolves over time), let us initially use the values given in Table 2 for 90 days in a moist room. A comparison between the estimated values on the basis of these data, and the experimentally obtained values (in terms of real beam compliance and real neutral axis position) will either verify or require rectification of this initial assumption taken for the Young’s moduli. The results are displayed in Table 4.

In the Batch 1 beams, the discrepancy between the calculated and the experimental results from Table 4 (columns 5 and 7 versus columns 8 and 9) is of minor importance in general, except for the IVP beam.

Hence, beams IP, ISC, and IVSC can be considered as well-performed and useful structural elements. In the IVP beam, the most visible difference appears to be the depth of the neutral axis (a real value of 147 mm versus a theoretical value of 118 mm) and, undoubtedly, the initially assumed elastic modulus of 31.4 GPa must be changed. Adjusting the calculations gave a more consistent value of E equal to 17 GPa, with n equal to 12, and the estimated values, x^{NA} , were equal to 141 mm and c was equal to 0.154 mm/kN, which were accepted as the closest approximation to the real mechanical characteristics of the IVP concrete mixture at the time of the bending test. Evidently, mixture IVP had not developed sufficient pozzolanic reactions before the start of the bending test. Had it done so, it might otherwise have had the stiffness value given in Table 2 (31.4 GPa) for specimens after 90 days in a moist room.

In the Batch 2a beams, the discrepancies between the calculations and the experimental results were also of minor importance, except in the case of the IIIP-M/25 beam. The other beams were well-performed structural elements, in which compliance was only slightly reduced following the use of fibers due to the increase of the water content in the fiber-reinforced concrete mixes. In the IIIP-M beam, the real position of the neutral axis (at a depth of 131 mm) yielded an n ratio of 15 units, with an elastic modulus, E , equal to 14 GPa, and a compliance value of 0.212 mm/kN, equal to the experimental value. Again, at the time of the bending test, the hydration of concrete in mixture IIIP-M had not reached the stiffness value given in Table 2 after 90 days in a moist room.

Finally, in the Batch 2b beams, the approach described in the above paragraph was followed, because the same concrete mixes as in Batch 2a were used. Therefore, the same can be said of beams IISC-M/16, IISC-Y/16 and IIIP-M/16, although some observations must be stated on the results of the IISC/16 beam. In this last case, the results were really poor in terms of compliance and neutral axis depth. The quality of the concrete in the upper region of this beam (compressed zone of concrete in the bending test) was clearly poor, yielding anomalous results (n equal to 20, and E equals 10 GPa) that may be neglected. An unexpected and undesired problem in the operation of concrete pouring, as sometimes

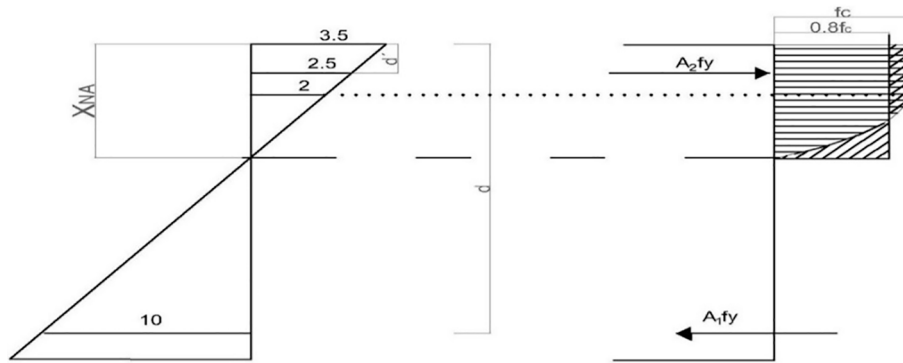


Fig. 6. Stress–strain schema of ideal failure within central sections of the beams.

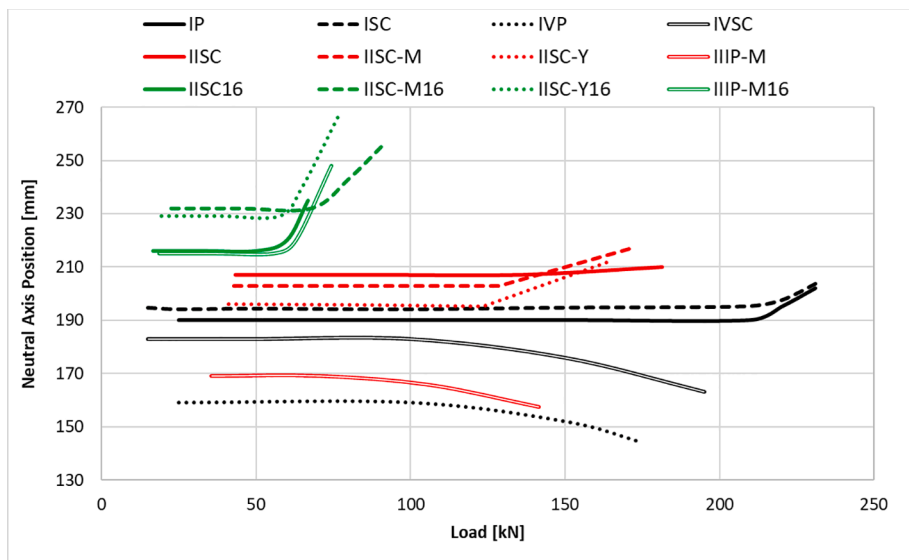


Fig. 7. Experimental evolution of the neutral axis position in the beams: a) Batch 1; b) Batch 2a; c) Batch 2b.

happens in construction practice, might offer some explanation. Therefore, the use of “safety coefficients” in concrete structural design is evidently indispensable.

4.4. Analysis of bending failure situation

The analysis of the failure moment when the strength of the beams gave way under increasing solicitation from external forces, *i.e.*, at the maximum load–deflection point, deserves extra comment. As previously mentioned, several “conventional” engineering standards base the design of reinforced concrete bending structures on a required factor of safety of two units, *i.e.*, the structure will be built to withstand twice the intended load, for reliable in-service behavior. Furthermore, the final collapse in the test is a consequence of static increases in bending forces when either the steel tensile bottom reinforcements yielded or when the concrete compressed zone yielded. In practice, both circumstances often occur simultaneously within well-designed beams.

In Fig. 6, a schematic stress–strain graph of the “simultaneous steel–concrete” moment of failure is shown. As the steel yields it reaches a strain close to 10‰ and the parabola–rectangle concrete stress regime is produced at strain levels of between 2 and 3.5‰. Although undoubtedly a simplification, it will help us to understand the analysis that is presented in the following paragraphs.

If the yield stresses for steel and for concrete are, respectively, f_y and f_c , and assuming an usual average value of concrete stress in the upper region of about $0.8f_c$, the equilibrium situation gave us the depth of the

neutral axis by Eq. (10), where b is the width of the concrete section. In our beams, b equals 200 mm, A_2 is always 100 mm^2 , and A_1 is equal to 1473, 982 and 402 mm^2 , for Batches 1, 2, and 3, respectively. The ratio between the mechanical strength of tensile steel and the compressed concrete is the key variable for calculation of the neutral axis depth (x^{NA}) at failure in each batch. That theoretical position of the neutral axis at failure is worth mentioning, because it differed from the position obtained in the former section under an elastic regime, which was dependent on the stiffness ratio (n , Eq. (7)) of the materials. The evolution in the depth of the neutral axis throughout the bending test was provided by the data collected from the corresponding strain gauges, which are depicted in Fig. 7 for all the beams under study.

$$x^{NA} = \frac{(A_1 - A_2) \cdot f_y}{0.8 \cdot f_c \cdot b} \tag{10}$$

The calculation of the ultimate bending moment in the plastic state of both materials (steel, concrete) was estimated with a formula derived from torques, Eq. (11), where, as in the former section, d is 260 mm and d' equals 26 mm, and the factor, 0.4, is derived from the position of the resultant force (center of gravity) on the compressed region. Once the depth of the neutral axis, described in the above paragraph, is established, the ultimate bending moment mainly depends on the yield stress of the steel in each batch. Finally, neglecting the effects of longitudinal top reinforcement (A_2) yields a simplified expression, Eq. (12), or, alternatively, Eq. (13). The results of the calculations using these simplified expressions are displayed in Table 5, and if compared with the

Table 5
Failure calculations.

Batch	BEAM	Initial estimation		Calculation results		Experimental data		Corrected values	
		28-day f_c (MPa)	f_y (MPa)	Neutral axis depth x^{NA} (mm)	Ultimate bending moment M_u (kN·m)	Neutral axis depth x^{NA} (mm)	Ultimate bending moment M_u (kN·m)	f_c (MPa)	
1 (3025)	IP	53	540	87	179	97	176	48	
	IVP	29	480 (*)	144	141	156	132	26	
	ISC	53	540	87	179	98	176	48	
	IVSC	31	490 (*)	135	148	137	146	31	
2a (2025)	IISC/25	59	640	75	147	90	138	46	
	IISC-M/25	53	600	66	139	83	129	40	
	IISC-Y/25	46	560	68	127	80	124	34	
	IIP-M/25	27	560 (*)	117	118	143	106	21	
2b (2016)	IISC/16	59	550 (*)	-	-	65	50	17	
	IISC-M/16	53	725 (*)	41	70	45	68	40	
	IISC-Y/16	46	600	39	66	33	58	34	
	IIP-M/16	27	590	40	60	52	56	21	

(*) values of steel stress at beam failure when $f < f_y$.

results of the building codes in Table 6, they are roughly convergent.

$$M_a = f_y \cdot [A_1 \cdot d - A_2 \cdot d' - 0.4 \cdot x^{NA} \cdot (A_1 - A_2)] \tag{11}$$

$$M_a = f_y \cdot A_1 \cdot d \cdot \left(1 - 0.4 \cdot \frac{x^{NA}}{d}\right) \tag{12}$$

$$M_a = f_y \cdot A_s \cdot d \cdot \left(1 - 0.5 \cdot \frac{A_s \cdot f_y}{b \cdot d \cdot f_{cm}}\right) \tag{13}$$

At this point, the yield strength of the reinforcing ribbed bar materials, f_y , must be established, before performing the static analysis at the failure moment. In the previous section “Rebars and fibers”, it was briefly stated that an initial, theoretical value of f_y equals 525 MPa could be used, corresponding to a strain level of 4.5‰, as computed in Eq. (1) in which E_s is 210 GPa. In the European standards (EC-2 code), the yield strength of B500SD steel is limited to under 1.25 times the nominal value (625 MPa). If the steel is simply qualified as B500S, as in our case, this limit does not exist, and the assumption is that the real f_y must be higher than 500 MPa, so the real steel yield strength could be noticeably higher.

Therefore, the envisaged failure analysis requires a reliable estimation of the yield strength of the steel, but detailed tensile tests were not performed on every bar, as is normal practice with materials engineered to certified specifications. Additionally, the reinforcement “cages” were provided by the suppliers on different dates over two years. Any uncertainty over the precise values of f_y can be approximately resolved from the data recorded by the strain gauges (G1 and G9) attached to the reinforcement bars, which provided valuable information for computing the steel stress or steel yield strength within each beam. This indirect method of estimating steel stress is based on the general formula of steel strain, Eq. (14), where e_o is the residual strain. Despite slight imprecisions, it is sufficient for our purpose. In Fig. 8, several graphs of these estimations are shown for each batch. The results of this analysis are depicted as f_y (MPa) in the fourth column of Table 5 where broad value ranges for the yield strengths of the tensile steel-ribbed bars can be observed.

$$e_s = e_o + \frac{f_s}{E_s} \tag{14}$$

The initial concrete strength estimates (specimens after 28 days in a moist room) are displayed in column 3 of Table 5. Subsequently, the results using the above-mentioned formulas for neutral axis position and ultimate moment are compared with the experimental data. Based on this comparison, corrected values of the real concrete strength of the beams submitted to bending tests were obtained and are displayed in the last column of Table 5.

Regarding Batch 1, Fig. 8a, it is worth mentioning that in the IVP and IVSC beams, the steel reinforcement bars hardly enter a state of yielding (marked with an asterisk in Table 5). Hence, the failure occurs due to the plasticization of the concrete in the upper region (where strain surpasses the standard values of 2–3.5‰), lowering the neutral axis of the sections with respect to the previous elastic state of loading, as shown in Fig. 7, in accordance with the predictions of the codes in Table 6. The stress state of tensile steel in these beams, at 480–490 MPa, deduced from Fig. 8a, approaches the non-linear zone of steel without net yielding, with strain values below the theoretical value of 4.5‰.

In the Batch 1 beams, IP and ISC, both the steel and concrete materials yielded at the failure moment, confirming the good design of these concrete sections, raising the neutral axis from the elastic regime to ultimate load (Fig. 7). Inverted calculations on the experimental results of all beams of this batch offer data from which the real strengths of the concrete mixtures in ultimate failure mode may be deduced. These results are displayed in the last column of Table 5. In general, these real concrete strength values for this batch are smaller than those obtained on specimens after 28 days in a moist room. The drop was in general close to 10%, except for the IVSC beam.

Table 6
Ultimate bending moments from standard calculation codes.

Batch	BEAM	Basic data			EC-2 code				ACI-318 standard	
		28-day f_c (MPa)	A_i (mm ²)	A_s (mm ²)	M_u (kN·m)	x (mm)	ϵ_c (‰)	ϵ_s (‰)	M_u (kN·m)	x (mm)
1 (3Ø25)	IP	53	1472.6	100.5	181.6	88	3.3	6.8	175.6	128
	IVP	29	1472.6	100.5	160.8	153	3.5	2.7	147.6	186
	ISC	53	1472.6	100.5	181.6	88	3.3	6.8	175.6	128
	IVSC	31	1472.6	100.5	164.3	143	3.5	3.1	150.6	177
2a (2Ø25)	IISC	59	981.7	100.5	127.5	59	2.7	10.0	121.3	82
	IISC-M	53	981.7	100.5	126.7	61	2.9	10.0	120.5	85
	IISC-Y	46	981.7	100.5	125.4	65	3.1	10.0	119.1	91
	IIIP-M	27	981.7	100.5	117.4	106	3.5	5.4	110.2	132
2b (2Ø16)	IISC	59	402.1	100.5	55.0	36	1.5	10.0	54.0	33
	IISC-M	53	402.1	100.5	54.9	36	1.5	10.0	53.9	35
	IISC-Y	46	402.1	100.5	54.8	37	1.6	10.0	53.6	37
	IIIP-M	27	402.1	100.5	53.7	50	2.2	10.0	52.1	54

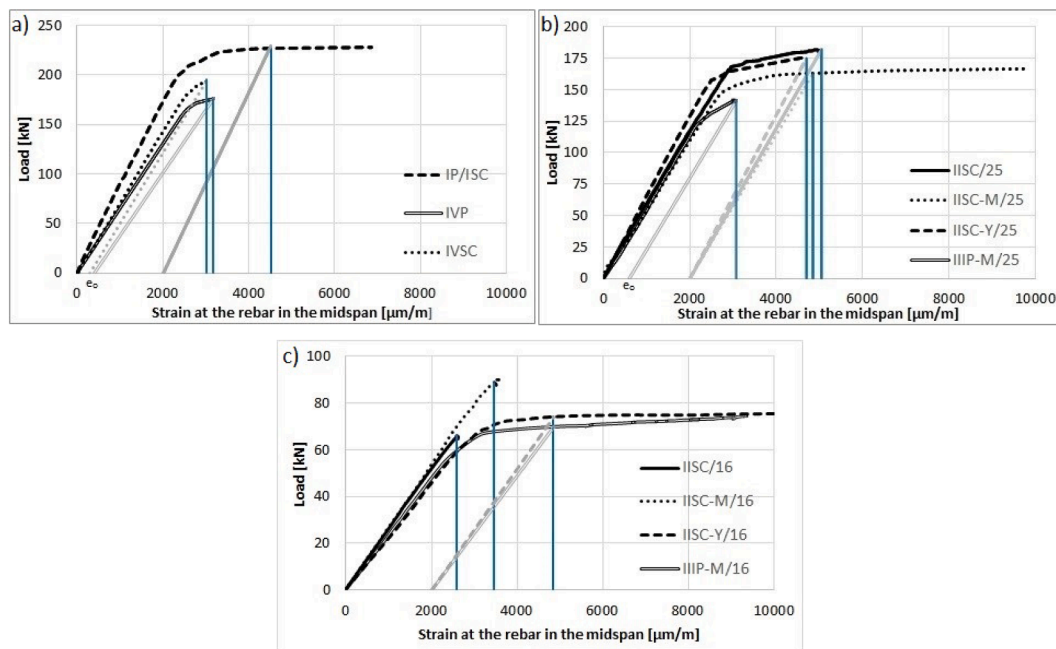


Fig. 8. Steel deformation: a) Batch 1; b) Batch 2a; c) Batch 2b. Strain under yield stress, or maximum strain, in blue. (For interpretation of the references to colour in this figure legend, the reader is referred to the web version of this article.)

In Batch 2a, the failure of the beams is produced with simultaneous yielding in both the steel and the concrete, except in the case of IIIP-M/25 beam. In this last case, the neutral axis is lower, due to the notable strain within the concrete, although the steel in the non-linear region had not yet to yield (as previously mentioned, in a similar way to IVP and IVSC), as depicted in Fig. 8b. After the backwards calculations, the corrected values for the concrete compressive strengths of this batch of beams were around 20% smaller with respect to the 28-day strength of the moist-room specimens. The effect of the fibers was no different under an elastic regime, so the ultimate bending moment of the beams with fibers was no greater, because the addition of fibers required a higher water content and the dilution of the cement was therefore higher.

In Batch 2b, beams IISC-Y/16 and IIIP-M/16 failed only after both materials yielded, as depicted in Fig. 8c for the steel. It is worth mentioning the singular situation which affected the other two beams. In the IISC/16 beam, an unexpected lack of concrete compressive strength explained its premature failure even though the steel had yet to yield. As in the previous section, this result can be neglected, due to the poor quality of the concrete.

The situation was also singular in the IISC-M/16 beam, in which the

steel yield strength was exceptional, almost 800 MPa, as may be deduced from the form of the corresponding curve shown in Fig. 8c. In this curve, the maximum stress, f_s , was 3.45 times 210 GPa, i.e., 725 MPa, and the steel never reached its yield point. Consequently, the maximum load of the bending test (90.5 kN) and the ultimate bending moment (68 kN·m) were unusually high for the reinforcement placed in this beam, in which the failure was due to concrete compression, despite the good quality of the concrete mix (40 MPa compressive strength).

4.5. Theoretical calculations according to the usual standards EC-2 code and ACI-318 standard

Table 6 depicts the main results of the standard calculation codes (European EC-2 code and ACI-318 standard) applied to the failure strength of the beams in a state of ultimate yield, which lost their bearing capacity. All calculations were based on the compressive strength of the concrete specimens conserved in the moist room for 28 days, the only measurements on the real material. In these calculations, the safety coefficients established by each regulation were also applied, except when referring to the properties of the materials, since they had been established in the experimental tests performed on the specimens

Table 7
Elastic calculations as per EC-2 code.

Batch	BEAM	28-day f_c (MPa)	E_c (GPa)	$n_{theoret}$	x (mm)	I_f (mm ⁴)	c (mm/kN)
1 (3025)	IP	53	36.3	5.5	123.4	3.07e + 08	0.109
	IVP	29	30.3	6.6	131.6	3.55e + 08	0.113
	ISC	53	36.3	5.5	123.4	3.07e + 08	0.109
	IVSC	31	30.9	6.5	130.6	3.49e + 08	0.113
2a (2025)	IISC	59	37.5	5.3	104.1	2.23e + 08	0.146
	IISC-M	53	36.3	5.5	105.4	2.26e + 08	0.149
	IISC-Y	46	34.8	5.8	107.1	2.34e + 08	0.150
	IIP-M	27	29.6	6.7	113.7	2.69e + 08	0.153
2b (2016)	IISC	59	37.5	5.3	70.8	1.12e + 08	0.290
	IISC-M	53	36.3	5.5	71.7	1.14e + 08	0.295
	IISC-Y	46	34.8	5.8	73.0	1.18e + 08	0.297
	IIP-M	27	29.6	6.7	77.9	1.38e + 08	0.298

and the test results of the beams. The main data were on the ultimate bending moment and the depth of the neutral axis, although the European code also specifies concrete strain in the upper (compressed) zone of the beams and the tensile strain of the lower steel reinforcements.

From this detailed information on EC-2 code, it may be appreciated that the failure of three beams (IVP, IVSC and IIP-M/25) was from the yielding of concrete, in which the strain within the steel never exceeded 5.5%. In the four beams of Batch 2b, the failure was preceded by the yielding of the steel reinforcement, with the concrete strain under 2.5%. Finally, yielding in both materials occurred at failure in the remaining five beams. This prediction was acceptable and in accordance with the experimental results.

In Table 7, the data are displayed in accordance with the European EC-2 code, analyzing the linear elastic state of the beams under notably lower loads than those at the point of failure. These data can be used to estimate beam stiffness against bending forces (EI , Young's modulus and moment of inertia), a magnitude that is indispensable to evaluate deflections and displacements within reinforced concrete structures. The most significant magnitude is the compliance of the beam (mm/kN), the inverse of its global stiffness (kN/mm).

The analyses shown in Table 7 were based on the calculations of the compressive strength of concrete specimens conserved in the moist room for 28 days, and the value of the modulus of elasticity was obtained with the corresponding formula. In general, the data on moments of inertia were reduced to concrete, and the n -ratio between the Young's moduli (steel to concrete) is the most important variable. The assumed depth of the neutral axis (x , mm) and the moment of inertia after tensile cracking (I_f , mm⁴) are displayed in the final two columns of Table 7. The values of compliance obtained through these calculations were slightly lower (higher stiffness) than those obtained from the analysis of the elastic regime of the beams.

In a summary, Table 8 shows the comparison between the calculation values according to the codes and the experimental results in the elastic regime and for the bending failure of the test beams. In general, a somewhat non-conservative adjustment between both values can be observed, underlining the advisability of using the experimentally obtained values of the mechanical properties to design structural elements with the mixtures that are under study.

5. Conclusions

The following conclusions may be advanced from the preparation of real-scale beams using pumpable and self-compacting concrete, in which the main component was electric arc furnace slag (EAFS), and their mechanical and bending testing.

- The actual bending strength of the beams was generally satisfactory, and the use of EAFS aggregate was a favorable factor in that assessment. The addition of large amounts of either ground

granulated blast-furnace slag (70%) or fly ash (50%) to the cement lowered the quality of the concrete. If the addition to cement is only 30% GGBS, the resultant concrete shares a similar quality with concrete cements without additions.

- The results of the bending tests, in terms of load versus deflection curves, showed linear elastic behavior up until loading levels of 80% of the ultimate failure load. Subsequently, a yield zone appeared, which quickly led to the failure of the beam. This behavior was independent of concrete composition.
- The presence of metallic or polymeric fiber reinforcement in some beams from Batches 2a and 2b were neither clearly favorable, nor detrimental, to the bending strength of the structural elements. The loss of workability and the subsequent increase in the water-to-cement ratio are detrimental against the improvement produced by fibers.
- The bending strength predictions of the design standards relating to the failure conditions of the beams were fairly precise, but slightly non-conservative, even though the starting point in their application was always the strength of the specimens after 28 days in a moist room.
- The experimental results and measures yielded estimates of the real values of compressive strength and the elastic modulus of each concrete mixture at the time of the tests, values that, in general, were lower than the strength and moduli measured after 90 days in a moist room.

These conclusions are based on the beams produced and tested in this study. Although manufactured with concrete mixes of different composition and mechanical characteristics, all the beams had fairly similar sizes and reinforcements, implying that the conclusions cannot be generalized. Further research in this field is therefore required, as it would be necessary to test the beams with different dimensions and reinforcements.

CRedit authorship contribution statement

Amaia Santamaría: Conceptualization, Methodology. **Aratz García-Llona:** Formal analysis, Validation. **Víctor Revilla-Cuesta:** Methodology, Data curation, Writing - review & editing. **Ignacio Piñero:** Data curation, Investigation. **Vanesa Ortega-López:** Resources, Writing - review & editing, Supervision, Project administration, Funding acquisition.

Declaration of Competing Interest

The authors declare that they have no known competing financial interests or personal relationships that could have appeared to influence the work reported in this paper.

Table 8
Comparison between theoretical and experimental results under an elastic regime and at failure.

Batch	BEAM	Elastic regime		Failure situation		Experimental ultimate bending moment (kN·m)
		Theoretical compliance (mm/kN)	Experimental compliance (mm/kN)	Theoretical ultimate bending moment (kN·m) (EC-2)	Theoretical ultimate bending moment (kN·m) (ACI-318)	
1 (3025)	IP	0.109	0.106	182	176	176
	IVP	0.113	0.152	161	148	132
	ISC	0.109	0.111	182	176	176
	IVSC	0.113	0.120	164	151	146
2a (2025)	IISC/25	0.146	0.157	128	121	138
	IISC-M/25	0.149	0.165	127	121	129
	IISC-Y/25	0.150	0.172	125	119	124
	IIP-M/25	0.153	0.212	117	110	106
2b (2016)	IISC/16	0.290	0.413	55	54	50
	IISC-M/16	0.295	0.310	55	54	68
	IISC-Y/16	0.297	0.340	55	54	58
	IIP-M/16	0.298	0.390	54	52	56

Acknowledgements

This work was supported by the Spanish Ministry MCI, AEI, EU and ERDF [RTI2018-097079-B-C31; 10.13039/501100011033; FPU17/03374]; the Junta de Castilla y León (Regional Government) and ERDF [UIC-231, BU119P17]; Youth Employment Initiative (JCyL) and ESF [UBU05B_1274]; the University of Burgos [grant number SUCONS, Y135.GI], UPV/EHU (PPGA20/26) and, finally, our thanks also go to the Basque Government research group IT1314-19 and likewise to CHRYSO and HORMOR for supplying the materials for research.

References

- [1] Our Common Future. Report of the World Commission on Environment and Development: Our Common Future, United Nations (UN). 1987.
- [2] Yu M, Robati M, Oldfield P, Wiedmann T, Crawford R, Nezhad AA, et al. The impact of value engineering on embodied greenhouse gas emissions in the built environment: A hybrid life cycle assessment. *Build Environ* 2020;168:106452. <https://doi.org/10.1016/j.buildenv.2019.106452>.
- [3] Palacios-Munoz B, Peuportier B, Gracia-Villa L, López-Mesa B. Sustainability assessment of refurbishment vs. new constructions by means of LCA and durability-based estimations of buildings lifespans: A new approach. *Build Environ* 2019;160:106203. <https://doi.org/10.1016/j.buildenv.2019.106203>.
- [4] Skaf M, Manso JM, Aragón A, Fuente-Alonso JA, Ortega-López V. EAF slag in asphalt mixes: A brief review of its possible re-use. *Resour Conserv Recycl* 2017;120:176–85.
- [5] Pasetto M, Baldo N. Experimental evaluation of high performance base course and road base asphalt concrete with electric arc furnace steel slags. *J Hazard Mater* 2010;181(1-3):938–48.
- [6] Pasetto M, Baldo N. Mix design and performance analysis of asphalt concretes with electric arc furnace slag. *Constr Build Mater* 2011;25(8):3458–68.
- [7] Yildirim IZ, Prezzi M. Use of steel slag in subgrade applications. Joint Transportation Research Program, Indiana Department of Transportation and Purdue University, West Lafayette, Indiana: Publication FWA/IN/JTRP-2009/32; 2009.
- [8] Bosela P, Delatte N, Obratil R, Patel A. Fresh and hardened properties of paving concrete with steel slag aggregate. *Carreteras* 2009;4(166):55–66.
- [9] Fronck B, Bosela P, Delatte N. Steel slag aggregate used in portland cement concrete. *Transp Res Rec* 2012;2267(1):37–42.
- [10] Liapis A, Anastasiou EK, Papachristoforou M, Papayianni I. Feasibility Study and Criteria for EAF Slag Utilization in Concrete Products. *J Sust Metal* 2018;4(1):68–76.
- [11] Santamaría A, Faleschini F, Giacomello G, Brunelli K, San José J-T, Pellegrino C, et al. Dimensional stability of electric arc furnace slag in civil engineering applications. *J Clean Prod* 2018;205:599–609.
- [12] Morino K, Iwatsuki E. Durability of concrete using electric arc furnace oxidizing slag aggregates. Sheffield, UK: Sheffield Academic Press; 1999. p. 213–22.
- [13] Roy S, Miura T, Nakamura H, Yamamoto Y. Investigation on applicability of spherical shaped EAF slag fine aggregate in pavement concrete – Fundamental and durability properties. *Constr Build Mater* 2018;192:555–68.
- [14] Faleschini F, Zanini MA, Pellegrino C, editors. New perspectives in the use of electric arc furnace slag as coarse aggregate for structural concrete. International Conference Euroslag; 2015; Linz, Austria.
- [15] Yildirim IZ, Prezzi M. Chemical, mineralogical, and morphological properties of steel slag. *Adv Civ Eng* 2011;2011:1–13.
- [16] Cho BS, Choi YC. Properties of cementless binders using desulfurization slag as an alkali activator. *J Ceram Process Res* 2018;19(1):37–42.
- [17] Fiol F, Thomas C, Muñoz C, Ortega-López V, Manso JM. The influence of recycled aggregates from precast elements on the mechanical properties of structural self-compacting concrete. *Constr Build Mater* 2018;182:309–23.
- [18] Revilla-Cuesta V, Skaf M, Faleschini F, Manso JM, Ortega-López V. Self-compacting concrete manufactured with recycled concrete aggregate: An overview. *J Clean Prod* 2020;262:121362. <https://doi.org/10.1016/j.jclepro.2020.121362>.
- [19] Brand AS, Roesler JR. Steel furnace slag aggregate expansion and hardened concrete properties. *Cem Concr Compos* 2015;60:1–9.
- [20] Brand AS, Roesler JR. Interfacial transition zone of cement composites with steel furnace slag aggregates. *Cem Concr Compos* 2018;86:117–29.
- [21] Jiang Yi, Ling T-C, Shi C, Pan S-Y. Characteristics of steel slags and their use in cement and concrete – A review. *Resour Conserv Recycl* 2018;136:187–97.
- [22] Manso JM, Hernández D, Losáñez MM, González JJ. Design and elaboration of concrete mixtures using steelmaking slags. *ACI Mater J* 2011;108(6):673–81.
- [23] Abu-Eishah SI, El-Dieb AS, Bedir MS. Performance of concrete mixtures made with electric arc furnace (EAF) steel slag aggregate produced in the Arabian Gulf region. *Constr Build Mater* 2012;34:249–56.
- [24] Etxeberria M, Pacheco C, Meneses JM, Berridi I. Properties of concrete using metallurgical industrial by-products as aggregates. *Constr Build Mater* 2010;24(9):1594–600.
- [25] Faleschini F, Alejandro Fernández-Ruiz M, Zanini MA, Brunelli K, Pellegrino C, Hernández-Montes E. High performance concrete with electric arc furnace slag as aggregate: Mechanical and durability properties. *Constr Build Mater* 2015;101:113–21.

- [26] Pellegrino C, Cavagnis P, Faleschini F, Brunelli K. Properties of concretes with black/oxidizing electric arc furnace slag aggregate. *Cem Concr Compos* 2013;37(1):232–40.
- [27] Pellegrino C, Gaddo V. Mechanical and durability characteristics of concrete containing EAF slag as aggregate. *Cem Concr Compos* 2009;31(9):663–71.
- [28] Polanco JA, Manso JM, Setién J, González JJ. Strength and durability of concrete made with electric steelmaking slag. *ACI Mater J* 2011;108(2):196–203.
- [29] Wang Y, Suraneni P. Experimental methods to determine the feasibility of steel slags as supplementary cementitious materials. *Constr Build Mater* 2019;204:458–67.
- [30] Yildirim IZ, Prezzi M. EAF Ladle Steel Slag as a Geo-Material: Compaction and Shear Strength Characteristics. *Geotech Spec Publ*; 2018. p. 113–22.
- [31] Qasrawi H. Towards sustainable self-compacting concrete: Effect of recycled slag coarse aggregate on the fresh properties of SCC. *Adv Civ Eng* 2018;2018:1–9.
- [32] Santamaría A, Orbe A, San José JT, González JJ. A study on the durability of structural concrete incorporating electric steelmaking slags. *Constr Build Mater* 2018;161:94–111.
- [33] Aragón G, Aragón Á, Santamaría A, Esteban A, Fiol F. Physical and mechanical characterization of a commercial rendering mortar using destructive and non-destructive techniques. *Constr Build Mater* 2019;224:835–49.
- [34] Santamaría A, Rojí E, Skaf M, Marcos I, González JJ. The use of steelmaking slags and fly ash in structural mortars. *Constr Build Mater* 2016;106:364–73.
- [35] Arribas I, San-José J, Vegas I, Hurtado J, Chica JA. Application of steel slag concrete in the foundation slab and basement wall of the Tecnalia kubik building. In: Proceedings of the 6th European Slag Conference Proceedings; 2010. p. 251–64.
- [36] Cho BS, Choi YC. Hydration Properties of STS-Refining Slag-Blended Blast Furnace Slag Cement. *Adv Mater Sci Eng* 2018;2018:5893254.
- [37] Skaf M, Ortega-López V, Fuente-Alonso JA, Santamaría A, Manso JM. Ladle furnace slag in asphalt mixes. *Constr Build Mater* 2016;122:488–95.
- [38] Netinger I, Rukavina MJ, Serdar M, Bjegović D. Steel slag as a valuable material for concrete production. *Teh Vjesn* 2014;21(5):1081–8.
- [39] Qasrawi H. Hardened properties of green self-consolidating concrete made with steel slag coarse aggregates under hot conditions. *ACI Mater J* 2020;117(1):107–18.
- [40] Navarro-Gregori J, Mezquida-Alcaraz EJ, Serna-Ros P, Echegaray-Oviedo J. Experimental study on the steel-fibre contribution to concrete shear behaviour. *Constr Build Mater* 2016;112:100–11.
- [41] Ortega-López V, Manso JM, Cuesta II, González JJ. The long-term accelerated expansion of various ladle-furnace basic slags and their soil-stabilization applications. *Constr Build Mater* 2014;68:455–64.
- [42] Serjun VZ, Mirtić B, Mladenović A. Evaluation of ladle slag as a potential material for building and civil engineering. *Mater Tehnologije* 2013;47(5):543–50.
- [43] Parron-Rubio ME, Perez-García F, Gonzalez-Herrera A, Rubio-Cintas MD. Concrete properties comparison when substituting a 25% cement with slag from different provenances. *Materials* 2018;11(6):1029.
- [44] Rebello TA, Zulcão R, Calmon JL, Gonçalves RF. Comparative life cycle assessment of ornamental stone processing waste recycling, sand, clay and limestone filler. *Waste Manage Res* 2019;37(2):186–95.
- [45] Roslan NH, Ismail M, Khalid NHA, Muhammad B. Properties of concrete containing electric arc furnace steel slag and steel sludge. *J Build Eng* 2020;28:101060. <https://doi.org/10.1016/j.jobbe.2019.101060>.
- [46] Kim S-W, Lee Y-J, Kim K-H. Flexural behavior of reinforced concrete beams with electric arc furnace slag aggregates. *J Asian Archit Build Eng* 2012;11(1):133–8.
- [47] Kim S-W, Lee Y-J, Lee Y-H, Kim K-H. Flexural performance of reinforced high-strength concrete beams with EAF oxidizing slag aggregates. *J Asian Archit Build Eng* 2016;15(3):589–96.
- [48] Lee Y-J, Kim H-G, Park J-H, Lee K-S, Kim K-H. Flexural behaviour prediction for RC beams in consideration of compressive stress distribution of concrete with electric arc furnace oxidising slag aggregates. *Eur J Environ. Civ Eng* 2020;24(5):689–708.
- [49] Kim S-W, Lee Y-J, Kim K-H. Bond behavior of RC beams with electric arc furnace oxidizing slag aggregates. *J Asian Archit Build Eng* 2012;11(2):359–66.
- [50] Faleschini F, Hofer L, Zanini MA, dalla Benetta M, Pellegrino C. Experimental behavior of beam-column joints made with EAF concrete under cyclic loading. *Eng Struct* 2017;139:81–95.
- [51] Pellegrino C, Faleschini F. Experimental behavior of reinforced concrete beams with electric arc furnace slag as recycled aggregate. *ACI Mater J* 2013;110(2):197–205.
- [52] Faleschini F, Santamaría A, Zanini MA, San José JT, Pellegrino C. Bond between steel reinforcement bars and electric arc furnace slag concrete. *Mater Struct* 2017;50(3):170.
- [53] Anastasiou EK, Papayianni I, Papachristoforou M. Behavior of self compacting concrete containing ladle furnace slag and steel fiber reinforcement. *Mater Des* 2014;59:454–60.
- [54] Pan Z, Zhou J, Jiang X, Xu Y, Jin R, Ma J, et al. Investigating the effects of steel slag powder on the properties of self-compacting concrete with recycled aggregates. *Constr Build Mater* 2019;200:570–7.
- [55] Fuente-Alonso JA, Ortega-López V, Skaf M, Aragón Á, San-José JT. Performance of fiber-reinforced EAF slag concrete for use in pavements. *Constr Build Mater* 2017;149:629–38.
- [56] Cuenca E, Echegaray-Oviedo J, Serna P. Influence of concrete matrix and type of fiber on the shear behavior of self-compacting fiber reinforced concrete beams. *Compos Part B: Eng* 2015;75:135–47.
- [57] Ortega-López V, Fuente-Alonso JA, Santamaría A, San-José JT, Aragón Á. Durability studies on fiber-reinforced EAF slag concrete for pavements. *Constr Build Mater* 2018;163:471–81.
- [58] Pujadas P, Blanco A, Cavalero SHP, de la Fuente A, Aguado A. Flexural post-cracking creep behaviour of macro-synthetic and steel fiber reinforced concrete. *RILEM Bookseries* 2017;14:77–87.
- [59] Faleschini F, De Marzi P, Pellegrino C. Recycled concrete containing EAF slag: Environmental assessment through LCA. *Eur J Environ Civ Eng* 2014;18(9):1009–24.
- [60] Pellegrino C, Faleschini F. Sustainability Improvements in the Concrete Industry: Use of Recycled Materials for Structural Concrete Production, Springer: Green Energy and Technology Serie. Green Energy and Technology Serie: Springer; 2016.
- [61] Saha AK, Khan MNN, Sarker PK. Value added utilization of by-product electric furnace ferronickel slag as construction materials: A review. *Resour Conserv Recycl* 2018;134:10–24.
- [62] Qasrawi H. The use of steel slag aggregate to enhance the mechanical properties of recycled aggregate concrete and retain the environment. *Constr Build Mater* 2014;54:298–304.
- [63] Lo Monte F, Ferrara L. Tensile behaviour identification in Ultra-High Performance Fibre Reinforced Cementitious Composites: indirect tension tests and back analysis of flexural test results. *Mater Struct* 2020;53(6):145.
- [64] Prasanna PK, Ramachandra Murthy A, Srinivasu K. Prediction of compressive strength of GGBS based concrete using RVM. *Struct Eng Mech* 2018;68(6):691–700.
- [65] Choi W-C, Yun H-D. Long-term deflection and flexural behavior of reinforced concrete beams with recycled aggregate. *Mater Des* 2013;51:742–50.
- [66] Yang JM, Kim JK. Development and application of a hybrid prestressed segmental concrete girder utilizing low carbon materials. *Struct Eng Mech* 2019;69(4):371–81.
- [67] Nwankwo CO, Ede AN. Flexural strengthening of reinforced concrete beam using a natural fibre reinforced polymer laminate: an experimental and numerical study. *Mater Struct* 2020;53(6):142.
- [68] European Committee for Standardization. Rue de Stassart, 36. Brussels B-1050.
- [69] Santamaría A, Orbe A, Losañez MM, Skaf M, Ortega-Lopez V, González JJ. Self-compacting concrete incorporating electric arc-furnace steelmaking slag as aggregate. *Mater Des* 2017;115:179–93.
- [70] Santamaría A, Ortega-López V, Skaf M, Chica JA, Manso JM. The study of properties and behavior of self compacting concrete containing Electric Arc Furnace Slag (EAFS) as aggregate. *Ain Shams Eng J* 2020;11(1):231–43.